Helimagnetism in XY models: Domain walls, frustrations, fractional vortices, and phase transitions

Gennadi Uimin[1,2,*] and Alberto Pimpinelli[2]

[1]*Laboratoire Leon Brillouin, Commissariat à l'Energie Atomique, Centre National de la Recherche Scientifique, Centre d'Études de Saclay, Saclay, F-91191 Gif-sur-Yvette, France*

[2]*Commissariat à l'Energie Atomique, Département de Recherche Fondamentale sur la Matière Condensée, Service de Physique Statistique, Magnetisme et Supraconductivité, Group de Magnetisme et Diffraction Neutronique, Centre d'Etudes Nucléaires de Grenoble, 17 Rue des Martyrs, F-38054 Grenoble Cedex 9, France*

(Received 24 May 1993)

We consider in this paper a model for two-dimensional XY helimagnets, which was proposed in Pimpinelli *et al.* [J. Phys. Condens. Matter **3**, 4693 (1991)]. In this model the usual spin waves and vortices coexist with chirality degrees of freedom in such a way that the degeneracy space of the order parameter is $O(2)\times Z_2$. In Pimpinelli *et al.* the low-temperature behavior of the model was addressed, and an infinite sequence of first-order phase transitions was shown to take place, due to the spin-wave coupling between domains with opposite chirality. Here we investigate the same model at higher temperatures, where vortices in the spin system and kinks on domain walls are thermally excited. The kinks in domain walls are associated with noninteger (fractional) vortices. This is presumably a common feature also in conventional helimagnets, where the Z_2 chirality is due to the twofold handedness of helices. We also discuss the applicability of this scenario to the helimagnetic compound $BaCo_2(AsO_4)_2$.

PACS number(s): 64.60.Cn, 75.10.Hk

I. INTRODUCTION

We will start by describing the main characteristics of the model of Ref. [1], which we will call XY(d) (d for decorated) model. It consists of an array of two-component classical spins (planar rotator model) sitting at the nodes of a decorated square lattice. The decoration is due to a spin situated at the center of each elementary square (plaquette) of the square lattice. The interactions are pairwise, each corner spin interacting with its four neighbors along plaquettes' sides, with vertical and horizontal coupling constants J_x and J_y, respectively, as well as with its four neighbors at the plaquettes' centers, with couplings J_1. Each decorating spin is also coupled to its two neighbors (in y direction) decorating spins with exchange J_2 (Fig. 1).

When plaquettes are decoupled ($J_2=0$) and one kind, say J_y, of the exchange integrals is chosen antiferromagnetic, the Hamiltonian allows for infinitely many lowest-energy states. This is due to the decoupling of the discrete chirality parameter in each column, so that chirality can take either value (± 1) in every column at the same energy cost. The cardinality of the degeneracy space is thus countable, as opposed to the more common degeneracy found in competing-interaction systems, where a continuum of degenerate states usually exists.

The degenerate phases are discussed in detail in [1]. Summarizing, we find two uniform phases, and a (countable) infinity of states obtained mixing in any arbitrary sequence domains of the uniform phases. These are a uniform helimagnetic phase, with wave vector $\mathbf{Q}=(1,\alpha)$, with $\cos\alpha=J_1/|J_y|$, where $\alpha/2$ is the angle between the corner and the central spin and a uniform ferrimagnetic state where the latter angle alternates in sign from corner to corner. An equivalent description may be obtained associating to each link parallel to the y axis the discrete, two-valued quantity (pseudo Ising spin) τ (see below), equal to the sign of the angle between adjacent corner spins in a plaquette. Then, we can assign to each and every phase in the degeneracy manifold a string of $+1$'s and -1's describing completely the relative phase. If the phase is uniform (collinear or modulated), the corresponding string has a definite periodicity, and it suffices to indicate the latter to characterize that particular state. For instance, in the helimagnetic phase α has the same sign on each link, so that the periodicity is infinite: we will use the axial next-nearest-neighbor Ising (ANNNI) model convention, and indicate this phase as $\langle\infty\rangle$. In the ferrimagnetic phase, α alternates from link to link, so

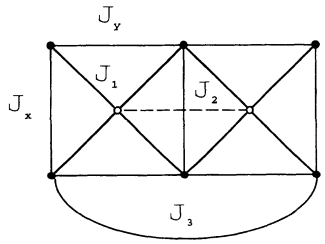

FIG. 1. Schematic representation of the couplings in the XY(d) model. Plaquettes can be coupled either through J_2 or J_3.

*On leave from Landau Institute for Theoretical Physics, ul. Kosygina 2, Moscow 117940, Russia.

that this phase is distinguished as $\langle 1 \rangle$. Degenerate with these two, we find all integer-modulation states, $\langle n \rangle$, n from 1 to ∞, long-period phases, $\langle \ldots nmpqr \ldots \rangle$, and completely aperiodic ones.

The set of zero-temperature degenerate states is therefore equivalent to the set of configurations of an anisotropic Ising model. The fictitious Ising spins have infinite interactions in the x direction, and vanishing coupling along y. The coupling is only introduced by temperature fluctuations of the real planar spins, so that the *free energy* of the original planar spin system can be *exactly* written, for $T \to 0$, as the *energy* of a fictitious Ising spin system, with T-dependent couplings. We were in fact able to compute this effective energy, which turns out to be

$$E(\{\tau\}) = E_0(T) + \frac{T^2}{2} \sum_{r,m} A_m \frac{1}{m^5} \tau_r \tau_{r+ma_y} , \tag{1}$$

where the coefficients A_m are all positive and asymptotically ($m \to \infty$) equal to the constant

$$A = \frac{3}{2^8 \pi^2 J_1^3 \cos^3(\alpha/2)} \frac{1}{(1+g_x)(1+g_y)^2} \times \left[\tilde{J}_y + \frac{1}{2} \tilde{J}_1 \left[1 + \frac{1+g_y}{1+g_x} \right] \right]^2 . \tag{2}$$

The ground state of this Ising model coincides thus with the low-temperature phase of the XY model. This ground state is now *unique,* and corresponds to the ferrimagnetic, $\langle 1 \rangle$ state. This finite-temperature selection of one state within a degeneracy manifold is by now well known ("order by thermal disorder").

As for all anisotropic Ising spin systems, the ground state of our model may also be described in terms of domain walls, separating domains where α takes opposite signs. At zero temperature the walls are noninteracting, and their interaction goes as T^2 at low $T > 0$. This interaction, which is due to spin-wave excitations, is repulsive, so that the wall system chooses the smallest nonvanishing possible distance.

The scenario that we have sketched above refers to uncoupled plaquettes. If we turn the interplaquette coupling J_2 on, the degeneracy is lifted and the lowest-energy state is either the ferrimagnet ($J_2 > 0$) or the helimagnet ($J_2 < 0$). In the latter case, a competition sets in between J_2 and spin waves, which would prefer the ferrimagnetic state. This competition gives rise, at low T and small J_2, to an infinite sequence of first-order phase transitions at increasing T, leading from $\langle \infty \rangle$ to $\langle 1 \rangle$, through all intermediate integer-period phases $\langle n \rangle$. The competing terms are proportional to $j_2 = J_2/J_1$ and $t^2 (t = T/J_1)$, respectively, so that the phase boundaries are straight lines in the j_2-t^2 plane.

Note that in a truly two-dimensional (2D) model the "phases" we mention are to be understood in the sense of states characterized by "quasi-long-range order," that is, by power-law decay of the correlation function. At higher temperatures, this behavior should transform into an exponential decay with a finite correlation length: It is the celebrated Kosterlitz-Thouless (KT) transition, due to topological excitations, called *vortices,* typical of the O(2) symmetry. Our model differs from a conventional planar one in two points. First, as we already mentioned, in the uncoupled-plaquette situation the symmetry of the order parameter is $U(1) \times Z_2$, so that the KT transition should be accompanied by Z_2, i.e., Ising-type, features, as a logarithmically singular specific heat, for instance. Second, another kind of excitation is present in the model, namely, *kinks* on the walls. Such kinks have the peculiarity, due to the background U(1) spins, that they are associated to *fractional vortices* [1], that is, to vortices of noninteger strength. We will discuss this point at length in the following sections.

Fractional vortices in magnetic models were a subject of interest since the mid 1980s: the possible occurrence of fractional vortices and the corresponding unbinding transitions have been suggested for a model with a special biquadratic exchange [2,3] and for Villain's odd model and homogeneously frustrated systems [4–6]. The latter case could be experimentally realized in 2D Josephson junction arrays and/or in ^{3}He-A films, were it not for definite experimental difficulties outside our current interest.

We will describe in this paper different scenarios, corresponding to different types of excitations and consequent transitions. They are, in brief, (1) compound vortex unbinding transition; (2) KT transition on an isolated domain wall; (3) floating-phase transition, caused by the fractional-vortex medium, in the system of domain walls; and (4) Ising-like phase transition on the $\langle 1 \rangle$-$\langle 2 \rangle$ phase boundary. We will then discuss the applicability of these scenarios to the XY helimagnet $BaCo_2(AsO_4)_2$ (see the review paper [7]), where some characteristics of the order-disorder transition may be determined by the competition of continuous and discrete degrees of freedom.

In the next section we will explicitly define the model Hamiltonian, and give some more detail on the low-T behavior. (We are not going to reproduce the long and tedious calculations performed in [1], and we refer to them if necessary. Some important formulas are nevertheless summarized in Appendix A.) In Sec. III we review the various topological excitations in connection with kinks and dislocations on the domain walls; in Sec. IV the possible phase transitions are described. Section V is for the discussion and conclusions.

II. THE MODEL HAMILTONIAN

It is time to introduce the reader to the characteristics of the model in even more detail.

First of all, a word on terminology. We have called the present model XY(d). In fact, we are considering planar rotators, that is, spins with only two components, with O(2) [U(1)] symmetry. The expression "XY model" should be reserved to three-component spins [SO(3) symmetry], with vanishing coupling between the third, S^z, say, spin components. Only in the latter case are out-of-plane fluctuations possible and the system has true dynamics. However, the two models are believed to belong to the same universality class, and to differ only quantitatively.

As we said, spins **S** are situated at the sites of a square

lattice, and are coupled ferromagnetically and antiferromagnetically in x and y direction, respectively. Moreover, the four spins in the elementary plaquette are effectively involved in a four-spin coupling via the interaction with a decorating spin σ at the center of the plaquette. In turn, the latter are coupled to the two neighbors in the y direction, with exchange J_2. The energy of the system can be written as follows:

$$E_0 = -\sum_r (J_x \mathbf{S}_r \cdot \mathbf{S}_{r+a_x} + J_y \mathbf{S}_r \cdot \mathbf{S}_{r+a_y}) - \sum_{\langle r,R \rangle} J_1 \mathbf{S}_r \cdot \boldsymbol{\sigma}_R - J_2 \sum_R \boldsymbol{\sigma}_R \cdot \boldsymbol{\sigma}_{R+a_y} , \quad (3)$$

where $J_x > 0$, $J_y < 0$, and, for definiteness, $J_1 > 0$. R and r denote sites on the decorating and main sublattices, respectively, and $\langle\ \rangle$ means nearest neighbors.

For $J_2 = 0$, the competition of opposite tendencies, i.e., to an antiferromagnetic arrangement along the y axis due to J_y and to a ferromagnetic one via the spins of the decorating sublattice, results in a spin rotation by an angle α [where $\phi(\mathbf{r}+\mathbf{a}_y)-\phi(\mathbf{r}) = \pm|\alpha|$ and $\cos\alpha/2 = J_1/|J_y|$], if $J_1 < |J_y|$. The ground state has a degeneracy of 2^N, where N is the number of rows (the degeneracy is therefore infinite in the thermodynamic limit). In other words, as we said, the energy cost of chiral domain walls is zero at $T = 0$.

At finite temperature the free energy may be written as an effective Hamiltonian for the chirality variables

$$\tau_r = \frac{\phi(\mathbf{r}+\mathbf{a}_y)-\phi(\mathbf{r})}{|\phi(\mathbf{r}+\mathbf{a}_y)-\phi(\mathbf{r})|}$$

in the form of Eq. (1). It is noteworthy that one may define the chirality variables as

$$\tau_r = \frac{\sin[\phi(\mathbf{r}+\mathbf{a}_y)-\phi(\mathbf{r})]}{|\sin[\phi(\mathbf{r}+\mathbf{a}_y)-\phi(\mathbf{r})]|} .$$

As we mentioned, Eq. (1) favors an "antiparallel" arrangement of the τ variables. A weakly antiferromagnetic J_2, however (a ferromagnetic J_2 would again favor the ferrimagnetic state), favors the homogeneous helimagnetic phase, with a helix pitch given as $\cos\alpha = J_1/|J_y + J_2|$. This interaction, which we rewrite here for clarity, acts in fact between spins at plaquette centers, along the y direction, that is

$$E_1 = -J_2 \sum_R \boldsymbol{\sigma}_R \cdot \boldsymbol{\sigma}_{R+a_y} . \quad (4)$$

We can explicitly show that this term induces a nearest-neighbor coupling of the chirality variables, τ's; to this end we approximate the spin product in Eq. (4) as follows:

$$\begin{aligned} \cos[\phi(\mathbf{R}+\mathbf{a}_y)-\phi(\mathbf{R})] &\approx \cos\left[\frac{\phi(\mathbf{r}+2\mathbf{a}_y)+\phi(\mathbf{r}+\mathbf{a}_y)}{2} - \frac{\phi(\mathbf{r}+\mathbf{a}_y)+\phi(\mathbf{r})}{2}\right] \\ &= \cos\left[\frac{\phi(\mathbf{r}+2\mathbf{a}_y)-\phi(\mathbf{r}+\mathbf{a}_y)}{2} + \frac{\phi(\mathbf{r}+\mathbf{a}_y)-\phi(\mathbf{r})}{2}\right] \\ &\to \cos^2(\alpha/2) - \sin^2(\alpha/2)\tau_r\tau_{r+a_y} . \end{aligned}$$

Thus a weak antiferromagnetic interaction in Eq. (4) together with the effective interaction via spin waves appears to be responsible for the phase transitions from the helimagnetic state at low temperatures (the sequence of spin rotations from row to row is either $\cdots + + + \cdots$ or $\cdots - - - \cdots$) to the high-temperature ferrimagnetic state where τ's alternate ($\cdots + - + - \cdots$). The system undergoes such a transition through infinitely many periodical phases:

$$\langle \infty \rangle \to \cdots \to \langle n+1 \rangle \to \langle n \rangle \to \langle n-1 \rangle \to \cdots \to \langle 2 \rangle \to \langle 1 \rangle ,$$

where any $\langle n \rangle$ structure includes alternating stripes of $+$'s and $-$'s, of constant width n:

$$\cdots (++\ldots++)(--\ldots--)\cdots ,$$

where there are n terms enclosed in each pair of parentheses. A qualitative sketch of the phase diagram is shown in Fig. 2. (See also Fig. 5 of Ref. [1].)

III. KINKS AND FRACTIONAL VORTICES

A fascinating feature of the XY(d) model is that any kink on a domain wall is simultaneously a fractional vortex. We illustrate it through a somewhat naive picture in

Fig. 3. Let us calculate the total spin rotation along a loop encircling a kink. We suppose $\phi(\mathbf{r}+\mathbf{a}_y)-\phi(\mathbf{r}) = \pm\alpha$ above/below the domain wall and $\phi(\mathbf{r}+\mathbf{a}_x)-\phi(\mathbf{r}) = 0$.

Without the kink, we would expect to get 0 or any integer multiple of 2π. However, we see that the formal sum

$$\sum_i [\phi(\mathbf{r}_{i+1})-\phi(\mathbf{r}_i)]$$

taken along the closed contour in Fig. 3 turns out to give 2α. In order to avoid the inconsistency, a fractional vortex of strength $-\alpha/\pi$ (in units of regular integer vortices) must be created around a kink. This results in a logarith-

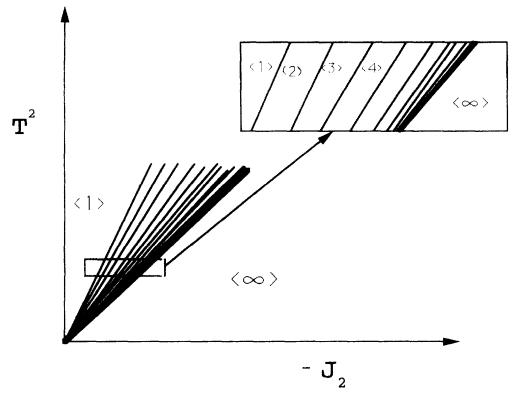

FIG. 2. Sketch of the low-temperature part of the phase diagram. In the T^2-J_2 plane the boundaries are straight lines, since the free energy difference contains terms proportional to T^2 and to J_2.

mic contribution to the kink self-energy. Similar considerations determine unambiguously the fractional vortex "charge" which depends on the chiralities below and above the domain wall and on the kink type. Four possible configurations are summarized in Fig. 4. Apart from the kinks, fractional vortices also appear on the dislocationlike domain-wall configurations which are represented in Fig. 5.

All the possibilities mentioned above are based on the following construction as illustrated in Fig. 6: (1) there are two adjacent rows which separate (from above and from below) areas of definite chirality; (2) a fractional vortex, situated between the two nearest rows, rotates a spin field (with respect to a certain background) along the contour $1\rightarrow 2\rightarrow 3\rightarrow 4\rightarrow 1$ by the angle $2\pi f$; (3) the contribution of chiralities is zero along both semicircles, $1\rightarrow 2$ and $3\rightarrow 4$; the nonzero contribution can be produced by the two pieces, $3\rightarrow 2$ and $4\rightarrow 1$, if their chiralities are opposite; it results in the total spin rotation caused by chiralities by the angle $\pm 2\alpha$. This construction covers all the cases shown in Figs. 4 and 5. It is very important to realize that $2\pi f = 2\alpha$ is defined modulo 2π, due to gauge invariance of the Hamiltonian [13]. In other words, the vortex charge is defined through the function $\{x\}$ as follows:

$$f = \left\{\frac{\alpha}{\pi}\right\} = \frac{\alpha}{\pi} - \text{nint}\left[\frac{\alpha}{\pi}\right], \tag{5}$$

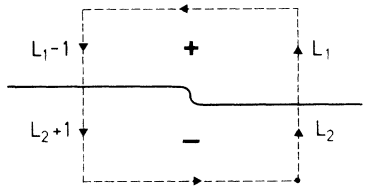

FIG. 3. A kink on a domain wall which separates two regions of negative (−) and positive (+) chiralities. The total misfit of spin orientation after going once around the contour is $[-L_2+L_1-(L_1-1)+(L_2+1)]\alpha = 2\alpha$.

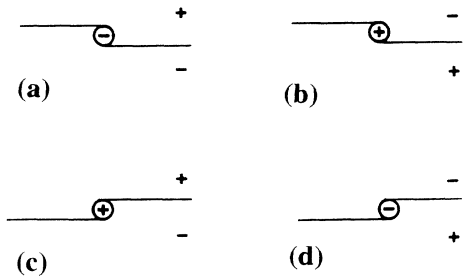

FIG. 4. Four possible configurations of fractional vortices, attached to domain walls, and corresponding chiralities.

where nint(x) is the nearest integer to x. Note that, according to this definition, $-\frac{1}{2} < \{x\} \leq \frac{1}{2}$.

We show fractional vortices schematically in Figs. 7 and 8. The spin fields depicted in Figs. 7 and 8 are equivalent to the kink and dislocationlike configurations of Figs. 4(a) and 5(a), respectively.

An important point is that fractional vortices are possible in conventional XY helimagnets where chirality is due to an *isotropic* competition of interactions. On the square lattice, for instance, the part of the energy responsible for helimagnetism has a form

$$E_{\text{hel}} = -J_1 \sum_{\mathbf{r}} (\mathbf{S}_r \cdot \mathbf{S}_{r+a_x} + \mathbf{S}_r \cdot \mathbf{S}_{r+a_y}) - J_3 \sum_{\mathbf{r}} (\mathbf{S}_r \cdot \mathbf{S}_{r+2a_x} + \mathbf{S}_r \cdot \mathbf{S}_{r+2a_y}) , \tag{6}$$

where $J_3 < 0$ and $|J_3|/4 \geq |J_1|$ (on the square lattice J_3 couples *third*-nearest neighbors). The addition of next-nearest-neighbor coupling J_2, with J_2 negative and $|J_2| \approx J_1/2$, allows for a helical ground state modulated in either the (1,0) or (0,1) directions. An additional Z_2 degeneracy is thus present in this case. A slightly anisotropic J_1 in (6) lifts this degeneracy and makes the problem completely equivalent to our own. However, at variance with the XY(d) model where the domain-wall width is one lattice spacing, an equilibrium domain-wall configuration generically involves a gradual change of the spin rotation angle from $-|\alpha|$ to $+|\alpha|$. On the other

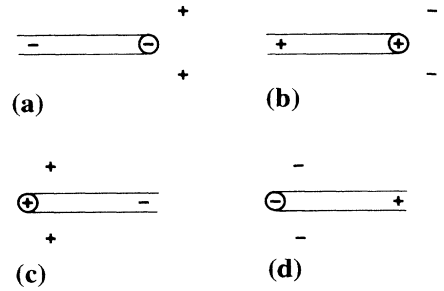

FIG. 5. Four possible configurations of fractional vortices, attached to dislocationlike domain walls, and corresponding chiralities.

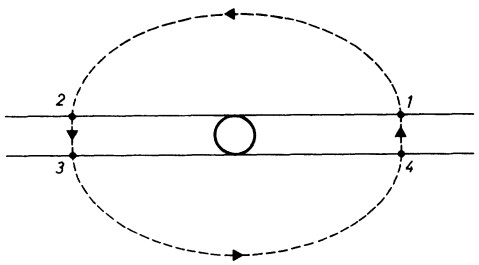

FIG. 6. See explanations in the text.

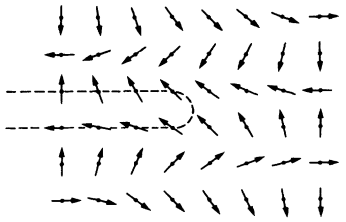

FIG. 8. Spin field of the fractional vortex of the charge $-\frac{1}{2}$, the analog of Fig. 5(a).

hand, this variation could be represented as a set of "minimal" domain walls separating regions of successive spin rotations

$$-\alpha|\cdots|\alpha_{-1}|\alpha_0|\alpha_1|\alpha_2|\cdots|\alpha\ .$$

Formally, a fractional vortex on a domain wall separating the areas $\alpha_j|\alpha_{j+1}$ has a charge $\pm(\alpha_{j+1}-\alpha_j)/2\pi$. These charges should decrease exponentially with $|j|$ and the total charge is again $\pm|\alpha|/\pi$. Coarse graining on the typical wall width, we would thus expect to obtain a picture similar to that in the present model.

A. Towards the fractional-vortex unbinding transitions

The logarithmic contribution to the self-energy of vortices, as well as to their interaction energy, can be found directly from the form of the spin Hamiltonian in the long-wavelength limit. The prelogarithmic factor enables us to perform quite reasonable estimates of the vortex unbinding temperature, of the helicity modulus, and of the critical exponents at the KT transition temperature. In the framework of the present model, the long-wavelength expansion of E_0 [Eq. (3)] has the following form:

$$E_0 \approx E_{\rm GS} + \tfrac{1}{2}\int d^2r[\tilde{J}_x(\partial_x\theta)^2+\tilde{J}_y(\partial_y\theta)^2]\ , \qquad (7)$$

where

$$\tilde{J}_x = J_x + J_1^2/|J_y|,\quad \tilde{J}_y = |J_y| + J_2 - J_1^2/|J_y|$$

from the ferrimagnetic side ($J_2>0$) and

$$\tilde{J}_x = J_x + J_1^2/(|J_y|+|J_2|)\ ,$$

$$\tilde{J}_y = |J_y|+|J_2| - J_1^2/(|J_y|+|J_2|)$$

from the helimagnetic side ($J_2<0$). The quantities θ are the angular deviations of the spins from their ground-state orientations, and $E_{\rm GS}$ is the ground-state energy.

The prelogarithmic factor in the fractional-vortex self-energy, which is computed from Eq. (7), differs from the corresponding value for an integer vortex, $\pi\sqrt{\tilde{J}_x\tilde{J}_y}$, by a factor $\{\alpha/\pi\}^2$. The inverse value of the universal jump of the helicity modulus as well as the critical exponents differ by the same factor. It also affects the estimate of the KT transition temperature, which would be

$$T_{\rm KT} \approx \frac{\pi}{2}K,\quad \text{where } K=\sqrt{\tilde{J}_x\tilde{J}_y}$$

if the system were not subjected to the fractional-vortex unbinding transition at a lower temperature, $T_{\rm FV}\approx T_{\rm KT}\{\alpha/\pi\}^2$.

B. Compound fractional vortices

However, even $T_{\rm FV}$ is not the lower theoretical limit for a transition in this system. Let us consider a compound fractional vortex of "double" charge $\{2\alpha/\pi\}$ [see definition of $\{x\}$ in Eq. (5)], consisting of two single vortices. It can be built as in Fig. 9. If $|\{2\alpha/\pi\}|<|\{\alpha/\pi\}|$, then the compound vortex medium undergoes an unbinding transition at a temperature

$$T_{\rm CV} \approx T_{\rm KT}\left\{2\frac{\alpha}{\pi}\right\}^2 .$$

Compound fractional vortices of smaller effective charges also can apparently be built up. First, one can assume that the core energy of the nth-order vortex, $\varepsilon_c(n)$, grows with n. Second, since it is logarithmically divergent, the self-energy of the compound vortex of the nth order can be written as $\varepsilon_v(n)\ln L$, where $\varepsilon_v(n)\propto\{n\alpha/\pi\}^2$. Hence we can establish a hierarchy,

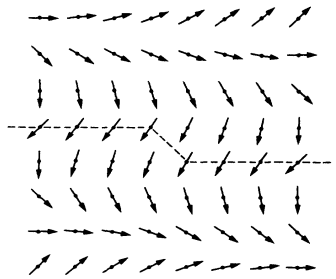

FIG. 7. Spin field of the fractional vortex of the charge $-\frac{1}{4}$, the analog of Fig. 4(a).

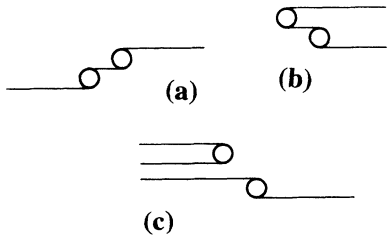

FIG. 9. Examples of fractional vortices of double vorticity attached to the same domain wall (a), (b) and to the nearest domain walls (c).

according to which only those compound vortices are effective whose charge satisfies the following inequalities:

$$\left|\left\{n\frac{\alpha}{\pi}\right\}\right| < \min\left[\left|\left\{\frac{\alpha}{\pi}\right\}\right|, \left|\left\{2\frac{\alpha}{\pi}\right\}\right|, \cdots, \left|\left\{(n-1)\frac{\alpha}{\pi}\right\}\right|\right]. \tag{8}$$

The selection according to the rule in Eq. (8) is illustrated in Fig. 10, where the compound vortex self-energy is shown vs $\ln R/r_0$. Doubtless, the higher the vortex order which satisfies the inequalities of Eq. (8), the smaller its energy in the thermodynamic limit. However, in a numerical or real experiment with a system of necessarily finite size, $\ln R/r_0$ cannot be larger than 20. This circumstance significantly restricts the set of candidates described in (8) which could be really observed in a numerical study of the model, or in a real system. In addition, the core energy of compound vortices grows with the number of the constituents, but it is not simply proportional to the total number of kinks involved in a compound vortex. For example, if two simple vortices are involved in a double vortex, satisfying the condition (8), the latter behaves on small distances as two simple fractional vortices plus an integer one, which compensates the double charge, $2\alpha/\pi$, if it falls out of the interval $(-1/2,1/2)$. The interaction energies of the constituents, separated by the distances r_{12}, r_{23}, and r_{13}, where 1 and 2 are the fractional vortices and 3 the integer one, may be written in the form

$$\varepsilon_c(2)=2\varepsilon_c+\varepsilon_c^{(i)}-\left[\frac{\alpha}{\pi}\right]^2\ln\frac{r_{12}}{r_0}+\frac{\alpha}{\pi}\left[\ln\frac{r_{23}}{r_0}+\ln\frac{r_{13}}{r_0}\right],$$

where $\varepsilon_c^{(i)}$ is the core energy of the integer vortex. We also note that ε_c can be estimated as proportional to $(\alpha/\pi)^2$ for small α. Therefore it appears that the actual observation of compound vortices is quite doubtful.

It could be of interest to illustrate with a concrete numerical example the competition of compound vortices, as described by the algorithm Eq. (8). Let us suppose that the primary fractional vortex is of the charge 0.416. The set of compound vortices satisfying inequalities (8) is as follows: 0.416(1), 0.168(2), 0.080(5), −0.008(12), etc. Estimating the logarithmic energy gain and the loss due to the core contribution, one finds that the compound vortex configuration of the fifth order would compete with the second order, were it not for the finite size of a realistic system. Actually, for the competition mentioned above to be effective the size of a system, L, should satisfy the inequality $\ln(L/r_0)\geq 150$.

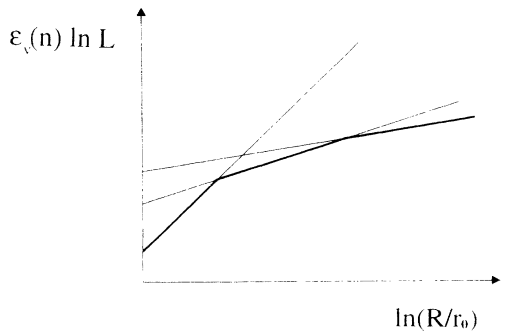

FIG. 10. The initial stage of the competition of fractional vortices vs the characteristic scale.

Concluding this section we briefly discuss the renormalization procedure applied to the medium of vortices with single and double charges. Details on the equations describing the evolution of the effective temperature K^{-1} and the bare fugacities y_1 and y_2 vs the rescaled lattice constant are given in Appendix B. [In such a renormalization procedure we follow José *et al.* [8].] The renormalization flows in the $y_1-y_2-K^{-1}$ space are mainly determined by the relevant y_2 coordinate, because the renormalized transition temperature T_{c2} due to double vortices is smaller than its single vortex counterpart. However, if the bare fugacity y_2 is small enough, a finite system could mimic the transition caused by single-charge vortices ($y_1\to 0$), which occurs at some renormalized temperature $T_1 < T_{c1}$. In fact, it is true that y_2 increases if $T_1 > T_{c2}$, but if the size of the system is insufficiently large there is the possibility that y_2 remains rather small.

Phase transitions due to compound vortices are certainly of great theoretical interest, but in the remainder of this paper we restrict ourselves to consideration of phenomena associated with the simplest fractional vortices.

IV. PHASE TRANSITIONS IN THE DOMAIN-WALL MEDIUM

We discuss now the effects of the vortex unbinding on the phase diagram of Fig. 2. We remind the reader that this phase diagram, obtained in [1], describes the set of transitions in the spin-wave interacting domain-wall medium, from the uniform helimagnetic state, which is mapped onto the *ferromagnetic* arrangement of (pseudo) Ising spins, $\langle\infty\rangle$, to the ferrimagnetic state, mapped onto $\langle 1\rangle$. Each striped phase, $\langle n\rangle$, is characterized by a concentration $1/n$ of domain walls. This concentration vanishes on the boundary between the set of striped phases and the helimagnetic region. We investigate in the following the modifications of Fig. 2 at higher temperatures, where topological excitations become effective. We distinguish three regimes, namely, low, intermediate, and high domain-wall concentrations. We will essentially follow this scheme: Going from one of the next three subsections to the following one, $|J_2|$ decreases, that is, we move on the phase diagram from $\langle\infty\rangle$ to $\langle 1\rangle$, while within each subsection J_2 is kept constant and the temperature is increased.

A. KT transition on the isolated domain wall

On the first-order [1] transition line separating the helimagnetic state from the set of ferrimagnetic states $\langle n\rangle$, the concentration of domain walls is zero, but a finite number of them does exist. We are therefore led to study

the behavior of an isolated domain wall.

At very low temperature the wall is straight, but kinks are thermally excited as T increases. The wall starts thus to fluctuate from row to row, each kink being accompanied by a fractional vortex. Note first of all that dislocationlike configurations—and the corresponding vortices (see Fig. 5)—are negligible, because these configurations are energetically too costly. As in ordinary KT transitions, at low temperature the constituents of the neutral fractional-vortex gas attached to the wall are bound in pairs. Hence the wall is localized. The vortex gas undergoes an unbinding transition (of the KT type) at

$$T_{1D} \approx 2 \left\{ \frac{\alpha}{\pi} \right\}^2 T_{KT} , \tag{9}$$

where the wall starts to diffuse freely, that is, it delocalizes. The factor 2 in Eq. (9) occurs because the entropy of a vortex attached to a (one-dimensional) wall is of a factor 2 smaller than the entropy of a vortex in the plane. These simple free energy arguments can be easily checked using scaling arguments. Actually, the partition function which includes spin-wave and fractional-vortex degrees of freedom can be mapped onto a sine-Gordon action, i.e., onto an action for spin waves in the presence of a symmetry-breaking cosine field [8]. In terms of the spin-wave variable θ's, such a field is of the form $\cos(2\pi K\{\alpha/\pi\}^2\theta)$. Its scaling dimensions would be (see, for example, [8,9]) $\lambda = 2 - \pi K\{\alpha/\pi\}^2$ in 2D, were it not for its reduced spatial dimensionality: In the present case, vortices are attached to a line—the domain wall—and thus live in an effectively 1D space. This circumstance transforms the eigenvalue λ of the symmetry-breaking field into $\lambda' = 1 - \pi K\{\alpha/\pi\}^2$.

B. Domain walls and possible transitions in intermediate phases

We now go a step further inside the phase diagram, where the $\langle n \rangle$ striped structures are stable at equilibrium. We suppose n to be moderate. Inside this structure dislocationlike excitations are very costly, and can be ignored. A kink on a wall now has two effects. First, it creates a fractional vortex with a logarithmical energy cost, as always. Second, it introduces a defect in the wall arrays, since beyond the kink the wall-wall separation is $n-1$ on one side and $n+1$ on the other. This defect has an energy cost proportional to the wall length on which it exists. Thus kinks will only occur in close pairs.

It is useful to describe this situation again in terms of domain walls. This time, however, we consider domain walls within the domain-wall medium. It is thus natural to speak of *secondary domain walls,* which are situated in coincidence with a "wrong" $n+1$ or $n-1$ interwall distance in a regular $\langle n \rangle$ structure. These secondary domain walls will be denoted as w_n^+ or w_n^- for $n+1$ or $n-1$ separation on an $\langle n \rangle$ background, respectively (Fig. 11). If we are inside the $\langle n \rangle$ phase, very close to the $\langle n \rangle$-$\langle n+1 \rangle$ phase boundary a w_n^+ secondary wall has a positive, but not large, free energy; we call it a *light wall.* On the other hand, in the same part of the phase diagram a w_n^- wall has a quite large positive free energy, and it will be termed *heavy* (Fig. 11). Of course, close to the $\langle n-1 \rangle$-$\langle n \rangle$ boundary the situation reverses: Now w_n^- is light and w_n^+ heavy.

In fact, we showed in [1] that all the $\langle n \rangle$-$\langle n+1 \rangle$ transition lines are first order, so that the two phases coexist at equilibrium there. Hence a finite number of light walls exists near such boundaries. These walls are very widely separate, so that we can treat them as isolated. As for primary walls, secondary walls fluctuate, creating kinks. However, kinks on secondary domain walls are not so costly in energy, because (see Fig. 11) each of them is associated to a kink on a primary wall, but in such a way that the corresponding fractional vortices have charges of alternating signs. If an even number of them exists, the resulting screening effect cancels the logarithmic divergence in the energy, so that at a high enough temperature the secondary walls fluctuate freely. Note that an important difference exists between the present situation and the isolated domain wall studied in the preceding subsection. In that case, vortices are also arranged in a one-dimensional fashion, but their charges need not be—and are not in general—alternating along the wall. This is instead always the case in the present situation.

We can thus consider the secondary domain wall as a one-dimensional gas of alternating charges $\pm f$, with logarithmic interactions—the fractional vortices of Fig. 11, aligned on the secondary domain wall as pearls on a necklace. Such a problem has been solved by Anderson, Yuval, and Hamann in the early 1970s [10]. We shortly outline their approach in Appendix C. Using the results of [10] we can estimate that unbinding of fractional vortices occurs above approximately $f^2 T_{KT}$.

The free energy per vortex can now be used in the calculation of the effective fugacity of a kink, z. From another point of view, z can be interpreted as the kinetic energy of a quantum particle in the framework of a transfer-matrix approach. In this framework a fluctuating wall is mapped to the space-time trajectory of a gas of free fermions, $\{c^\dagger, c\}$, with Hamiltonian

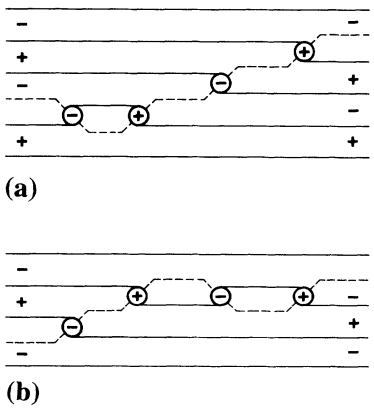

FIG. 11. (a) Mapping of a secondary domain wall onto a 1D set of fractional vortices. (b) One of the manifold configurations after application of the inverse mapping. Secondary domain walls are shown as dashed lines.

$$H=\frac{\Delta_n^+}{T}\sum_i c_i^\dagger c_i - z\sum_i (c_i^\dagger c_{i+1}+\text{H.c.})\ , \tag{10}$$

where Δ_n^+ is the self-energy per unit length of the secondary domain wall, as computed in Appendix A [see Eq. (A5)]. Note that z can be roughly estimated through the vortex core energy, and that the latter does not vanish at zero temperature, its finite limit being a function of the relevant exchange constants, J_x, J_y, J_1, and J_2. On the contrary, the domain-wall energy is proportional to T^2, for both primary and secondary walls, and thus vanishes with T. The phase transition from the low-temperature phase with straight—on average—secondary domain wall into the high-temperature phase where the wall propagates diffusively in the plane (as in the case of the isolated domain wall), occurs at a temperature which can be evaluated by equating the kinetic and the self-energy. It is thus given by

$$2z(T_{\rm fl}^{(n,n+1)})=\frac{\Delta_n^+(T_{\rm fl}^{(n,n+1)})}{T_{\rm fl}^{(n,n+1)}}\ . \tag{11}$$

Note that at low but finite temperature the $\Delta_n^\pm$'s are positive. Hence, for all temperatures below $T_{\rm fl}^{(n,n+1)}$, defined by Eq. (11), a secondary domain wall is energetically unfavorable. At $T_{\rm fl}^{(n,n+1)}$ the free energy of w_n^+ secondary domain walls vanishes, to become negative at higher temperatures. Thus secondary domain walls proliferate, and start to interact; the competition of the single-wall energy gain with the repulsive interwall interaction leads to the setting in of the so-called floating phase (fl), characterized by quasi-long-range order in the diluted gas of $\langle n+1\rangle$ pieces on the regular $\langle n\rangle$ background. Since this transition is of the Pokrovsky-Talapov type [11], the concentration of secondary domain walls varies with temperature as $\sqrt{T-T_{\rm fl}^{(n,n+1)}}$.

The transitions into the floating phase of w_n^+ walls on the $\langle n\rangle$ background and the transition of w_{n+1}^- walls on the $\langle n+1\rangle$ background are not symmetrical: The critical temperature of the former is higher than that of the latter, as we explicitly show in Appendix A [see Eqs. (A8) and (A9)]. This implies that at the critical temperature $T_{\rm fl}^{(n,n+1)}$, which lies on the first-order $\langle n\rangle$-$\langle n+1\rangle$ transition line, the concentration of ω_{n+1}^- domain walls stays finite, while that of w_n^+ vanishes continuously. At this point the boundary splits with a cusplike behavior (see Fig. 12). Beyond $T_{\rm fl}$ the $\langle n\rangle$-fl transition is continuous, while the $\langle n+1\rangle$-fl transition is first order: Along this part of the boundary the transition proceeds from the regular chiral structure into the floating chiral structure with a finite concentration of secondary domain walls. The point determined by Eq. (11) appears thus to be a tricritical point, where a second-order and a first-order line meet. Upon further increasing the temperature, the $\langle n+1\rangle$-fl transition also becomes continuous at a second tricritical point (Fig. 12).

Note that in fact there are two boundaries dividing, say, the $\langle n\rangle$ phase from the floating phase: We denote them $\langle n\rangle^+$-fl and $\langle n\rangle^-$-fl, since they originate from the $\langle n\rangle$-$\langle n+1\rangle$ and $\langle n-1\rangle$-$\langle n\rangle$ first-order transition lines, respectively. As it is clear from the topology of the phase diagram in Fig. 12, these two boundaries must meet at some T. This temperature should lie on the geometrical locus of points of the n-modulated region, where the energies of the two types of secondary walls involved, w_n^+ and w_n^-, coincide. This locus certainly exists, because, as we said above, the w_n^+ walls are heavy (with reference to their energy cost, see above) and w_n^- walls are light near the $\langle n\rangle^-$-fl boundary, whereas they exchange their role near the $\langle n\rangle^+$-fl line. We would speculate that this meeting point of the phase boundaries is a critical point in the universality class of the spin $S=1$ quantum chain with planar anisotropy (for details of the transfer-matrix approach in analogous problems see [12]). This point will be further addressed in a separate paper.

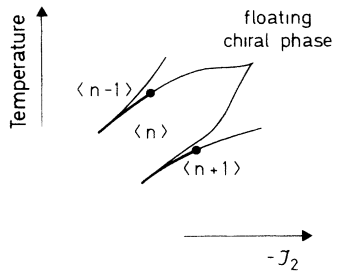

FIG. 12. Fragment of the phase diagram in the J_2-T plane. The first-order transition lines are thick, the continuous transitions into floating phase are shown in thin lines.

C. Phase transitions on the ⟨1⟩-⟨2⟩ boundary

This case differs from the previous one because the ferrimagnetic $\langle 1\rangle$ phase has, besides fractional vortices, Ising-like excitations in the form of solitons (2α soliton). This point has been also briefly considered in [1]. In other words, together with the kinklike excitations on the domain walls, described in the transfer-matrix formalism by the kinetic energy term of free fermions, there exists a relevant contribution, describing the creation (annihilation) process of two fermions. Although the fugacity of such an excitation is smaller than that of the one shown in Fig. 11, the process of creation (annihilation) of a dislocation in the case under discussion is relevant, because a dislocation only consists of two "fermions." Actually, considering the general case of the fermion creation from the background $\langle n\rangle$ (wrong pieces $\langle n\pm 1\rangle$), one obtains the total number of constituents (secondary domain walls) of the simplest dislocation loop being equal to $2n$. Kosterlitz and Thouless [14] derived a criterion for stability of a solid against formation of free dislocations. It states that the solid is stable if $p^2\geq 8$, where p is related via $|\mathbf{b}|=pa$ to the minimum Burgers vector $\mathbf{b}$ of the dislocations. Applying this criterion to our case with $p=2n$, we conclude that the inequality $(2n)^2\geq 8$ is not satisfied only for the phase $\langle 1\rangle(n=1)$, so that the transition from this phase to the floating one is forbidden. It undergoes instead an Ising-like transition directly to the disordered (paramagnetic) state [1].

In Fig. 13(a) we show the spin configuration which characterizes one type of 2α soliton. In terms of the pri-

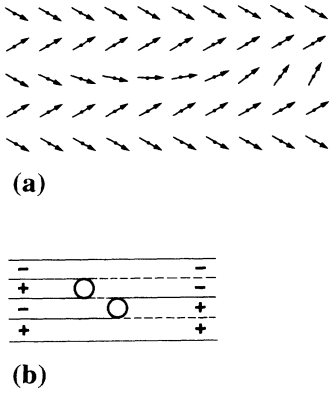

FIG. 13. 2α soliton on the $\langle 1 \rangle$ background; (a) spin configuration; (b) equivalent dislocationlike configuration, emphasizing primary domain walls (solid lines), secondary domain wall (dashed line), and fractional vortices.

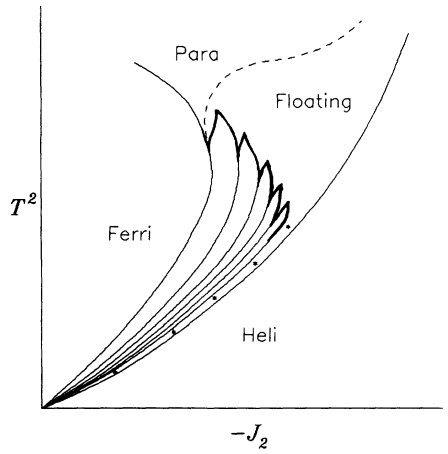

FIG. 14. Qualitative sketch of the complete phase diagram of the model, as resulting from the discussion of Sec. IV.

mary and secondary domain walls and the fractional vortices, the soliton is equivalent to the excitation sketched in Fig. 13(b). This is a dislocationlike configuration of the secondary domain wall. Because of the two fractional vortices forming the core of the dislocation, its fugacity is $z_d \ll z$. Described in the framework of the transfer-matrix method by means of fermionic variables, the equivalent Hamiltonian is a generalization of Eq. (10):

$$H=\frac{\Delta_1^+}{T}\sum_i c_i^\dagger c_i - z\sum_i (c_i^\dagger c_{i+1}+\text{H.c.}) - z_d\sum_i (c_i^\dagger c_{i+1}^\dagger+\text{H.c.})\ . \tag{12}$$

Although the phase-transition line is formally the same as given by Eq. (11), the physical content is different due to the last term in Eq. (12), i.e., the statistical model corresponding to the 1D quantum Hamiltonian of Eq. (12) is the anisotropic Ising model.

Again, the phase equilibrium line $\langle 1 \rangle$-$\langle 2 \rangle$ splits in a nonsymmetrical way: the part of the cusp from the $\langle 2 \rangle$ phase side corresponds to the modulated-floating transition, as found generically and as shown in Fig. 12. In the proximity of the $\langle 1 \rangle$ phase, the quasi-long-range-ordered floating phase transforms into a disordered state. A similar behavior has been found for the 2D ANNNI model by Villain and Bak [15]. However, the possibility also exists that the transition line separating the disordered and floating phase ends at the tricritical point on the $\langle 2 \rangle$-fl boundary line. For the reader's convenience we summarize all our results in Fig. 14, which contains a sketch of the complete phase diagram of the model.

V. DISCUSSIONS AND CONCLUSION

Fractional vortices and domain walls, to which vortices are attached, are topologically available in systems with nonzero chiralities. Among other representatives helimagnets should be mentioned. In this paper we give the rule to construct a fractional vortex which is either a kinklike or a dislocationlike configuration on a domain wall. Its "charge" is determined unambiguously through chiralities and topological properties of kink and/or dislocation.

Certainly, the topological excitations like domain walls and fractional vortices influence each other. From one side, fractional vortices cannot exist outside domain walls. On the other hand, they drive the domain-wall critical behavior.

Summarizing our results, we have extended to higher temperatures the investigation of the model of Ref. [1]. The resulting phase diagram, in the region of the coupling constant space where the model's ground state has helimagnetic and ferrimagnetic spin arrangements, exhibits the following features.

(1) An infinite set of spin-wave-induced first-order phase transitions from the helimagnetic state ($\langle \infty \rangle$—chiralities are "ferromagnetically" ordered) to the ferrimagnetic state ($\langle 1 \rangle$—"antiferromagnetic" ordering of chiralities).

(2) Each line of two-phase equilibrium $\langle n+1 \rangle$-$\langle n \rangle$ splits at some finite temperature, forming a cusp, with appearance of the intermediate floating phase between the two lines. The system undergoes the continuous floating-phase transition from the side of the $\langle n \rangle$ phase, whereas the line of the first-order phase transition continues beyond the triple point, separating the $\langle n+1 \rangle$ and floating phases, and transforms into the line of continuous floating transitions.

(3) An exception to this general scheme occurs on the boundary $\langle 2 \rangle$-$\langle 1 \rangle$ where the line splitting is accompanied by the appearance of a branch of the Ising-like transition into the phase in which secondary domain walls on the $\langle 1 \rangle$-background are disordered. There are no principal changes in the phase-transition picture from the side of the $\langle 2 \rangle$ phase as compared with the general scheme. It is nonetheless clear that disordered and floating states must be separated by another phase-transition line.

The situation in more traditional—that is, with isotropic Hamiltonians—helimagnets seems to be not so exciting as in the XY(d) model, because there is no special smallness of the domain-wall energy. In other words, in

the XY(d) model fractional vortices have a significant effect upon the chiral floating-disordering transitions. The possible phase transitions in traditional helimagnets, as mentioned in the Introduction, could be analyzed in the style of Ref. [5]. Unfortunately, such a general analysis cannot give an unambiguous answer about the sequence of the phase transitions and their universality classes (see, also, discussion in [4]). We would like anyway to mention that our model is not so academic as it might seem; we have already shown in [1] that it is possible to perform exactly the statistical trace over the decorating spins at plaquettes' centers, when they are not coupled, so that one obtains an effective, temperature-dependent Hamiltonian involving only spins on a simple square lattice. The price to pay is that spins within a plaquette are now coupled also through a four-spin interaction, of the form

$$\beta|J_1||\mathbf{S}_1+\mathbf{S}_2+\mathbf{S}_3+\mathbf{S}_4| ,$$

where 1 to 4 index the spins on the elementary square. Note, however, that at low temperature we may approximate the absolute value by its square. Since spins are constrained to unit length, $|\mathbf{S}_i|^2=1$, the square of the total spin of the plaquette is exactly rewritten in terms of two-spin couplings only:

$$\beta|J_1|\left[4+2\sum_{(i<j)=1}\mathbf{S}_i\cdot\mathbf{S}_j\right] . \tag{13}$$

The resulting Hamiltonian hence contains nearest ($\tilde{J}_1^x,\tilde{J}_1^y$) and next-nearest- ($\tilde{J}_2$) neighbor couplings of the form

$$\tilde{J}_1^x=-J_x+2\beta|J_1| ,$$
$$\tilde{J}_1^y=-J_y+2\beta|J_1| ,$$
$$\tilde{J}_2=2\beta|J_1| .$$

If we now couple third-nearest neighbors in this simple square lattice, we get for the Hamiltonian the more familiar form

$$\tilde{H}=-\sum_i(\tilde{J}_1^x\mathbf{S}_i\cdot\mathbf{S}_{i+a_x}+\tilde{J}_1^y\mathbf{S}_i\cdot\mathbf{S}_{i+a_y})-\tilde{J}_2\sum_i(\mathbf{S}_i\cdot\mathbf{S}_{i+a_x+a_y})$$
$$-\tilde{J}_3\sum_i(\mathbf{S}_i\cdot\mathbf{S}_{i+2a_x}+\mathbf{S}_i\cdot\mathbf{S}_{i+2a_y}) . \tag{14}$$

Actually, this (effective) Hamiltonian is exact if the decorating spins are taken as continuous variables instead of XY spins, since then a Gaussian integration over these variables leads to Eqs. (13) and (14). As we said before, the anisotropy in nearest-neighbor couplings lifts the degeneracy between (1,0)- and (0,1)-directed helices [16].

Finally, we outline the very intriguing experimental situation (see [7], and references therein) which originated our interest in topological excitations in helimagnets.

$BaCo_2(AsO_4)_2$ is a quasi-2D XY helimagnet. Responsible for the magnetic properties are the spin-$\frac{1}{2}$ Co ions which are arranged in the honeycomb lattice structure. The relevant exchange constants, derived from the spin-wave dynamics, involve nearest-neighbor as well as third-nearest-neighbor spins. The low-temperature magnetic structure can be suitably represented as two compenetrating triangular sublattices with helix wave vector $\mathbf{Q}=(0.265,0)$, in units of 2π.

The regular spin rotation angle from one sublattice to the other is less than 15°. The transition temperature appears to be approximately $\frac{1}{4}$ of a nominal KT integer vortex unbinding transition. In spite of the well-defined Bragg peak at the helix wave vector $\mathbf{Q}$, the spin-wave excitation displays overdamping around $\mathbf{q}\approx\mathbf{Q}$. However, its "optical" branch is propagative and shows a gap $\Delta_0\approx 1.5$ meV at $\mathbf{q}=0$ which contrasts with the estimate $\Delta_0\approx 3$ meV, obtained from the specific heat measurements. Also, the fitting of the specific heat curve shows a T^2 behavior below 2 K, which indicates the existence of the Goldstone mode in the spectrum ($\omega_q\sim|\mathbf{q}-\mathbf{Q}|$). In addition, the specific heat singularity around T_c is too strong to be related to the KT transition exclusively: domain walls must be involved, at least.

So, the experimental problem still awaits a detailed analysis, which should also involve Monte Carlo simulations. We will report on them later. As a preliminary estimate we would like to speculate that the unusual temperature of the vortex unbinding transition could be associated with a gas of fractional vortices of vorticity $\approx\frac{1}{2}$, attached to randomly distributed domain walls, separating regions of opposite chiralities. This is not inconsistent with the information concerning dynamical excitations. Actually, the excitations which contribute to the thermodynamics could be fractional vortex-antivortex pairs, coupled in "quasimolecules." Both constituents are attached to domain walls. On the other hand, one considers a single fractional vortex in the image of the 2α soliton, propagating along the domain wall without damping. Therefore we need to assume that a randomly distributed domain-wall network enters the scene. However, the reason for its existence is not yet clear.

ACKNOWLEDGMENTS

The authors would like to thank J. Rossat-Mignod for his permanent interest in this work and L. P. Regnault for many stimulating discussions. A.P. acknowledges financial support from the CEE under the contract Science 915190. G.U. collaborated in this work during his stay in Grenoble and Saclay in the frame of the Ecole Normale Superieure–Landau Institute cooperation.

APPENDIX A

We use here formulas concerning wall-wall interactions that were derived in [1]. One can easily check that the self-energy of a single domain wall against the helimagnetic background is

$$\varepsilon_w=-2\sum_{p=1}^{\infty}pA_p , \tag{A1}$$

where A_p is defined in the text. Note that $A_1<0$ and $A_p>0$ ($p\geq 2$).

The interaction of domain walls separating the areas of opposite chiralities is not so easy to compute. We quote the result of Ref. [1]:

$$F_n^{(m)}=(-1)^{m-1}f_n,\quad f_n=4\sum_{p=1}^{\infty}pA_{n+p}\ . \tag{A2}$$

In Eq. (A2) n denotes a distance between two walls, whereas $(m-1)$ indicates how many domain walls are situated between them. Equation (A2) shows that the wall-wall interaction is not reduced to a two-body potential. The effective attraction of the next-nearest walls results in a simple sequence of phase transitions from the helimagnetic to ferrimagnetic state through infinitely many intermediate states according to the following scheme:

$$\text{helimagnet}=\langle\infty\rangle\rightarrow\cdots\rightarrow\langle n\rangle\rightarrow\cdots\rightarrow\langle 1\rangle=\text{ferrimagnet}\ .$$

Within the region of the phase diagram where one periodical configuration $\langle n\rangle$ is stable, we can define secondary domain walls, w_n^+ and w_n^-, coinciding with stripes of widths $n+1$ and $n-1$, respectively. The energy of a secondary domain wall is positive even on the lines of phase equilibrium $\langle n+1\rangle$-$\langle n\rangle$ and $\langle n\rangle$-$\langle n-1\rangle$. Below we explicitly derive the energies of different types of walls for the former case.

The $\langle n\rangle$-$\langle n+1\rangle$ phase-transition line is defined by the following equation:

$$\frac{1}{n}\left[\varepsilon_w+\sum_{p=1}^{\infty}(-1)^{p-1}f_{pn}\right]=\frac{1}{n+1}\left[\varepsilon_w+\sum_{p=1}^{\infty}(-1)^{p-1}f_{pn+p}\right], \tag{A3}$$

whereas the energy of a secondary domain wall w_n^+ is given by the expression

$$\Delta_n(w_n^+)=-\frac{1}{n}\left[\varepsilon_w+\sum_{p=1}^{\infty}(-1)^{p-1}f_{pn}\right]+\sum_{p=1}^{\infty}(-1)^{p-1}p(f_{pn+1}-f_{pn})\ . \tag{A4}$$

Substituting ε_w from Eq. (A3) into Eq. (A4) one obtains the energy of the w_n^+ wall on the line of $\langle n\rangle$ and $\langle n+1\rangle$ phase coexistence:

$$\Delta_{n,n+1}(w_n^+)=\sum_{p=1}^{\infty}(-1)^{p-1}\times[pf_{pn+1}-(p-1)f_{pn}-f_{pn+p}]\ . \tag{A5}$$

Performing the analogous calculations for $\Delta_{n,n+1}(w_{n+1}^-)$, i.e., the energy of secondary domain wall w_{n+1}^- on the line of the $\langle n\rangle$-$\langle n+1\rangle$ phase boundary, we obtain

$$\Delta_{n,n+1}(w_{n+1}^-)=\sum_{p=1}^{\infty}(-1)^{p-1}\times[pf_{pn+p-1)}-(p-1)f_{pn+p}-f_{pn}]\ . \tag{A6}$$

It may be of interest to compare these results with the energy of the w_n^- secondary wall, which can be interpreted as a light wall on the boundary $\langle n-1\rangle$-$\langle n\rangle$ and which plays the role of a heavy wall on the $\langle n\rangle$-$\langle n+1\rangle$ equilibrium line:

$$\Delta_{n,n+1}(w_n^-)=\sum_{p=1}^{\infty}(-1)^{p-1}\times[pf_{pn-1}-(p+1)f_{pn}+f_{pn+p}]\ . \tag{A7}$$

Performing the large-n expansion and keeping in mind that $f_n\propto n^{-k}$ ($k=4$ in two dimensions) we get

$$\Delta_{n,n+1}(w_{n+1}^-)\approx\Delta_{n,n+1}(w_n^+)\propto\frac{k(k+1)}{2n^{k+2}}\sum_{p=2}^{\infty}\frac{(-1)^p(p-1)}{p^{k+1}}\ , \tag{A8}$$

$$\Delta_{n,n+1}(w_n^-)\propto\frac{k(k+1)}{2n^{k+2}}\sum_{p=1}^{\infty}\frac{(-1)^{p-1}(p+1)}{p^{k+1}}\ . \tag{A9}$$

Comparing estimates from Eqs. (A8) and (A9) we conclude that the energy cost of light walls is much smaller numerically.

The curious peculiarity of Eqs. (A5) and (A6) is that although $\Delta_{n,n+1}(w_{n+1}^-)$ and $\Delta_{n,n+1}(w_n^+)$ coincide in the main order [see Eq. (A8)], they are not identical:

$$\Delta_{n,n+1}(w_n^+)-\Delta_{n,n+1}(w_{n+1}^-)=\sum_{p=1}^{\infty}(-1)^{p-1}[p(f_{pn+1}-f_{pn+p-1})+(p-2)(f_{pn+p}-f_{pn})] \tag{A10}$$

but differ from each other beginning at $p=3$.

APPENDIX B

This appendix is for deriving the renormalization group equations. The derivations follow the general scheme performed in [8].

We consider the case of two kinds of incommensurate vortices which are referred to in Sec. II A as vortices of the single and double charges. The partition function can be suitably decoupled into the spin-wave part and the part due to vortices (we omit all the contributors except single and double fractional vortices):

$$Z(y_1,y_2)=Z_{sw}Z_v(y_1,y_2)\ . \tag{B1}$$

For the spin-wave partition function we use the conventional $x-y$ symmetrical form:

$$Z_{sw}=\left[\prod_r\int_{-\infty}^{+\infty}\frac{d\theta(\mathbf{r})}{2\pi}\right]\exp\left[-\frac{K}{2}\sum_r[\nabla\theta(\mathbf{r})]^2\right]\ . \tag{B2}$$

Concerning the action of vortices it can be written as

$$A_v\{m_1,m_2\}=\sum_r n_1^2(\mathbf{r})\ln y_1+\sum_r n_2^2(\mathbf{r})\ln y_2 + \sum_{\langle r_1,r_2\rangle} 2\pi K m(\mathbf{r}_1)G(\mathbf{r}_1-\mathbf{r}_2)m(\mathbf{r}_2)\ , \tag{B3}$$

where $n_{1,2}(\mathbf{r})$ is the "charge-occupation" number of fractional vortices, single and double, taking the values -1, 0, and $+1$. $m(\mathbf{r})$ can be expressed as

$$m(\mathbf{r})=m_1 n_2(\mathbf{r})+m_2 n_2(\mathbf{r})\ . \tag{B4}$$

Both vortex subsystems are supposed to be neutral, i.e., $\sum_r n_1(\mathbf{r})=\sum_r n_2(\mathbf{r})=0$. $G(r)$ behaves as $\ln r/r_0$ at distances much longer than the core size, r_0. Supposing the small-fugacity case to be correct for a true reproduction of the critical behavior, we perform a kind of low-temperature expansion for a gas of vortices. In such approximation the two groups of vortices of single and double fractional vorticities can be treated as independent because of the incommensurability, in general, of their charges.

The spin-wave contribution to the irreducible spin-spin correlation function like

$$\langle e^{i(\theta-\theta')}\rangle$$

is

$$g_{sw}=\exp[-G(\mathbf{r}-\mathbf{r}')/2\pi K]\ ,$$

whereas the contribution due to vortices is

$$g_v^{(i)}=\exp[-\pi G(\mathbf{r}-\mathbf{r}')m_i^2\Sigma_i/4]\ ,$$

$$\text{where } \Sigma_i=m_i^2\sum_r\langle n_i(0)n_i(r)\rangle \quad (i=1,2)\ .$$

Besides, Σ_i can be estimated as $-2y_i^2\exp[-2\pi KG(r)m_i^2]$.

These correlation functions are the basis for performing the traditional renormalization procedure according to which the following renormalization group (RG) equations can be obtained:

$$\frac{dK^{-1}}{dl}=2\pi^3(m_1^2y_1^2+m_2^2y_2^2)\ , \tag{B5}$$

$$\frac{dy_1}{dl}=(2-\pi m_1^2K)y_1\ , \tag{B6}$$

$$\frac{dy_2}{dl}=(2-\pi m_2^2K)y_2\ . \tag{B7}$$

APPENDIX C

Here we discuss how the floating transition occurs at the boundary of two-phase equilibrium $\langle n\rangle$-$\langle n+1\rangle$. As mentioned in Appendix A, the free energy Δ_n^+ of the secondary domain wall is positive even on the line of the $\langle n\rangle$-$\langle n+1\rangle$ phase equilibrium. The possibility for a domain wall to migrate comes from the kinklike excitations which are simultaneously fractional vortices. The physical meaning of the floating transition lies in the vanishing of the free energy of a single secondary domain wall. If one neglects all kinks resulting in heavy secondary walls, the floating transition problem can be reduced to the statistical mechanics of a collection of alternating charges on a line, interacting via a logarithmic potential. Anderson, Yuval, and Hamann [10] were the first who applied the renormalization group methods to the problem of a neutral "one-dimensional Coulomb gas."

Recall that the secondary domain wall is simply a stripe with "wrong" width $(n+1)$ within the regular structure of the primary domain walls spaced a distance n apart. Any secondary domain wall can be unambiguously mapped onto a one-dimensional set of fractional vortices (an example is shown in Fig. 11). The inverse transformation is ambiguous: any set of m vortices generates 2^m different secondary domain-wall configurations. The average distance between such vortices is reasonably supposed to be much larger than the lattice constant. In any case, a single domain wall propagates diffusively due to the kinks. Thus these allow us to treat the interaction of vortices with a good accuracy as dependent only on their x coordinates. With such assumptions the partition function of the isolated secondary domain wall has the form

$$Z=\sum_n \mathcal{T}^{2n}\int_0^L dx_{2n}\int_0^{x_{2n}-a} dx_{2n-1}\cdots\int_0^{x_2-a} dx_1 \exp\left[g\sum_{\substack{i,j\\ i>j}}(-1)^{i-j}\ln\left[\frac{x_i-x_j}{a}\right]\right]\ , \tag{C1}$$

where $\mathcal{T}=2\exp(-\varepsilon_c/T)$ is the fugacity of vortex cores; a is a cutoff of the order of the lattice constant. In Eq. (C1) the sum runs over n vortex pairs. Taking the partition function in the form of Eq. (C1) with alternative charges, we suppose that all kinds of heavy domain walls can be neglected. The origin of the factor 2, entering $\mathcal{T}$, is explained above; ε_c plays the role of the core energy; g involves the bare exchange constants and temperature, it is in fact proportional to $1/T$. According to the analysis of Ref. [10] the 1D neutral vortex plasma undergoes an unbinding transition when renormalized constant g becomes smaller than 2. What they perform is a renormalization *ante litteram*, which results in formulas completely analogous to the Kosterlitz-Thouless renormalization equations which appear, for instance, also at the end of the preceding Appendix.

[1] A. Pimpinelli, G. Uimin, and J. Villain, J. Phys. Condens. Matter **3**, 4693 (1991).
[2] D. H. Lee and G. Grinstein, Phys. Rev. Lett. **55**, 541 (1985).
[3] D. H. Lee, G. Grinstein, and J. Toner, Phys. Rev. Lett. **56**, 2318 (1986).
[4] T. C. Halsey, J. Phys. C **18**, 2437 (1985).
[5] S. E. Korshunov and G. V. Uimin, J. Stat. Phys. **43**, 1 (1986).
[6] S. E. Korshunov, J. Stat. Phys. **43**, 17 (1986).
[7] L. P. Regnault and J. Rossat-Mignod, in *Magnetic Properties of Layered Transition Metal Compounds,* edited by L. J. De Jongh (Kluwer, The Netherlands, 1990), pp. 271–321.
[8] J. V. José, L. P. Kadanoff, S. Kirkpatrick, and D. R. Nelson, Phys. Rev. B **16**, 1217 (1977).
[9] V. L. Pokrovsky and G. V. Uimin, Phys. Lett. **45A**, 467 (1973); Zh. Eksp. Teor. Fiz. **65**, 1691 (1973) [Sov. Phys. JETP **38**, 847 (1974).
[10] P. W. Anderson, G. Yuval, and D. R. Hamann, Phys. Rev. B **1**, 4464 (1970).
[11] V. L. Pokrovsky and A. L. Talapov, Phys. Rev. Lett. **42**, 2457 (1979).
[12] G. V. Uimin and V. L. Pokrovsky, J. Phys. (Paris) **44**, 865 (1983); L. A. Bol'shov, V. L. Pokrovsky, and G. V. Uimin, J. Stat. Phys. **38**, 191 (1985).
[13] E. Fradkin, B. A. Huberman, and S. H. Shenker, Phys. Rev. B **18**, 4789 (1978).
[14] J. M. Kosterlitz and D. J. Thouless, in *Progress in Low Temperature Physics,* edited by D. F. Brewer (North-Holland, Amsterdam, 1978); see also S. N. Coopersmith, D. S. Fisher, B. I. Halperin, P. A. Lee, and W. F. Brinkmann, Phys. Rev. Lett. **46**, 549 (1981).
[15] J. Villain and P. Bak, J. Phys. (Paris) **42**, 657 (1981).
[16] E. Rastelli, A. Tassi, and L. Reatto, Physica B **97**, 1 (1979).